



HAL
open science

Half-life determination of ^{215}At and ^{221}Ra with high-purity radioactive ion beams

S Bara, E Jajčičinová, T.E Cocolios, B Andel, S Antalic, A Camaiani, C Costache, K Dockx, G.J Farooq-Smith, A Kellerbauer, et al.

► **To cite this version:**

S Bara, E Jajčičinová, T.E Cocolios, B Andel, S Antalic, et al.. Half-life determination of ^{215}At and ^{221}Ra with high-purity radioactive ion beams. *Applied Radiation and Isotopes*, 2024, 208, pp.111289. 10.1016/j.apradiso.2024.111289 . hal-04521896

HAL Id: hal-04521896

<https://hal.science/hal-04521896v1>

Submitted on 18 Nov 2024

HAL is a multi-disciplinary open access archive for the deposit and dissemination of scientific research documents, whether they are published or not. The documents may come from teaching and research institutions in France or abroad, or from public or private research centers.

L'archive ouverte pluridisciplinaire **HAL**, est destinée au dépôt et à la diffusion de documents scientifiques de niveau recherche, publiés ou non, émanant des établissements d'enseignement et de recherche français ou étrangers, des laboratoires publics ou privés.

Half-life determination of ^{215}At and ^{221}Ra with high-purity radioactive ion beams

S. Bara^{a,1,*}, E. Jajčičinová^{a,b,2,*}, T.E. Cocolios^{a,*}, B. Andel^c, S. Antalic^c, A. Camaiani^{d,e,a}, C. Costache^f, K. Dockx^a, G.J. Farooq-Smith^{g,a}, A. Kellerbauer^b, R. Lica^f, K.M. Lynch^h, P. Mariniⁱ, M. Piersa-Silkowska^{j,k}, S. Stegemann^{j,a}, M. Stryczyk^{l,m,a}, D. Treasaⁱ, P. Van Duppen^a

^a*KU Leuven, Instituut voor Kern- en Stralingsfysica, 3001, Leuven, Belgium*

^b*European Commission, Joint Research Centre (JRC), Karlsruhe, Germany*

^c*Department of Nuclear Physics and Biophysics, Comenius University in Bratislava, 84248, Bratislava, Slovakia*

^d*Dipartimento di Fisica, Università di Firenze, I-50019, Sesto Fiorentino, Italy*

^e*Istituto Nazionale di Fisica Nucleare, Sezione di Firenze, I-50019, Sesto Fiorentino, Italy*

^f*Horia Hulubei National Institute for Physics and Nuclear Engineering, RO-077125, Bucharest, Romania*

^g*Department of Oncology Physics, Edinburgh Cancer Centre, Western General Hospital, Edinburgh, United Kingdom*

^h*School of Physics and Astronomy, The University of Manchester, M13 9PL, Manchester, United Kingdom*

ⁱ*University of Bordeaux, CNRS, LP2I, UMR 5797, F-33170, Gradignan, France*

^j*CERN, CH-1211, Geneva 23, Switzerland*

^k*Faculty of Physics, University of Warsaw, PL 02-093, Warsaw, Poland*

^l*University of Jyväskylä, Department of Physics, Accelerator laboratory, P.O. Box 35, FI-40014 University of Jyväskylä, Finland*

^m*Helsinki Institute of Physics, University of Helsinki, P.O. Box 64, FI-00014 Helsinki, Finland*

Abstract

At CERN-ISOLDE, high-purity radioactive ion beams of ^{219}Fr and ^{221}RaF were investigated with α -decay spectroscopy at the CRIS and ASET experiments in the course of three different experimental campaigns. The half-life of ^{215}At , α -decay daughter of ^{219}Fr , is measured to be $36.3(3)[9] \mu\text{s}$, and that of ^{221}Ra was determined to be $26.2(1)[6] \text{s}$, both of which are well in line with the trends in this region of the nuclear landscape but at odds with some of the reported literature.

1. Introduction

The region north-east of ^{208}Pb with $Z > 82$, $N > 126$ is well known for its very short-lived isotopes, down to μs and ns half-lives for ground states, due to the inherently fast α decay of these isotopes. While these short-lived isotopes are not too exotic, in the sense that they are not very far from ^{208}Pb , their study is hampered by their half-lives and limited to facilities that can investigate them within those time scales. However, many of them may also be produced along the decay chain of longer-lived, heavier radionuclides. For example, ^{219}Fr and ^{215}At , with sub-second half-lives, are part of the decay chain of ^{227}Pa , with a half-life of $38.3(3) \text{min}$, through a sequence of several α decays (Meinke et al., 1951; Graeffe and Kauranen, 1966; Bastin et al., 1968). In Meinke et al. (1951) the electronics had limited time resolution, thus, it could only measure half-lives in the range from $50 \mu\text{s}$ to 50ms .

The motivation to re-investigate this topic arose from a discrepancy between a recent measurement and the previously measured values. While attempting to explore the low-lying states in ^{219}Ra and ^{215}Rn with the TASISpec decay station at TASCAs, GSI, Sămark-Roth *et al.* were

also able to study the α -decay of some neighbouring decay chains, like those originating from ^{219}Fr and ^{221}Ra (Sămark-Roth et al., 2018). The energy and time information were extracted using a specifically developed pulse shape analysis routine and the different decay chains were studied using triple α coincidence analysis. A value of $37(3) \mu\text{s}$ was obtained for the half-life of ^{215}At , which substantially deviates from the previously measured value of $100(20) \mu\text{s}$ (Meinke et al., 1951; Singh et al., 2013). For ^{221}Ra , a half-life of $16(2) \text{s}$ was determined, compared to $30(2) \text{s}$ (Meinke et al., 1951) and $28(2) \text{s}$ (Tove, 1958; Kumar Jain et al., 2007) reported in the literature. Those are not the first half-lives in the region being questioned. For example, the half-life of the very short-lived ^{216}Ra was recently remeasured, suggesting a shorter value than previously reported from $182(10) \text{ns}$ to $161(11) \text{ns}$ (Sun et al., 2017; Parr et al., 2019).

Those isotopes are part of decay chains that may be of relevance in the production of medical radionuclides: ^{221}Ra is part of the decay chain of ^{225}Ac via a small β -decay branch in ^{221}Fr ($b_{\beta} < 0.10\%$ from Valli (1964)), while ^{215}At is part of the ^{223}Ac decay chain, which may be co-produced with ^{223}Ra . In order to properly interpret the analysis of the production rates and contaminants (see e.g. Johnson et al. (2023)), it is essential to have access to accurate half-life values. We thus proceeded in an independent investigation of those half-lives, based on existing data and new mea-

*Corresponding author

¹silvia.bara@kuleuven.be

²erika.jajcisinova@student.kuleuven.be

measurements with high-purity radioactive ion beams (RIB) at CERN-ISOLDE.

2. Experimental methods

At ISOLDE the RIB is produced by impinging a proton beam at 1.4 GeV and $2\ \mu\text{A}$ on average, onto a solid UC_x target. The isotopes of interest, namely ^{219}Fr ($T_{1/2} = 20(2)\ \text{ms}$) and ^{221}Ra ($T_{1/2} = 28(2)\ \text{s}$), are produced by spallation of uranium. The reaction products are then extracted by maintaining the target at a high temperature (typically around $2000\ \text{°C}$) and ionized through surface ionization, which is very efficient to produce Fr^+ and Ra^+ . The ions are then accelerated to an energy of 30–60 keV and analyzed through a dipole magnet to select a single mass of interest. This allows the production of a pure beam of ^{219}Fr , as isobaric ^{219}Ra is too short-lived ($T_{1/2} = 10\ \text{ms}$) to be efficiently extracted.

However, at $A = 221$, both ^{221}Fr and ^{221}Ra may be extracted together. Given the small β -decay branch of ^{221}Fr to ^{221}Ra , it is not possible to study the half-life of the latter as it is constantly fed by the decay of the former. When a fluorine-rich molecule is injected in the target, it is possible to produce other simple fluorinated molecules. This process enables the production of RaF^+ molecular beams, while Fr cannot be taken out in this form (Au et al., 2023). As a consequence, pure samples of ^{221}Ra may be obtained at a mass setting of $A = 221 + 19 = 240$.

At the end, a pure beam of the isotope of interest is produced and afterwards delivered to the experimental setup for one of three experimental campaigns, using either the Decay Spectroscopy Station (DSS) of the Collinear Resonance Ionization Spectroscopy (CRIS) experiment (IS471), or the Alpha SETup (ASET) to perform decay-spectroscopy studies (IS637 and IS665).

2.1. IS471: CRIS experimental campaign

The CRIS experiment is dedicated to high-resolution laser spectroscopy of radioactive isotopes and radioactive molecules (Cocolios et al., 2013; de Groote et al., 2015). Its initial scientific programme (2010–2015) was concentrated on the francium isotopic chain, presenting results ranging from ^{202}Fr to ^{231}Fr (Flanagan et al., 2013; Budinčević et al., 2014).

The detection setup of the CRIS experiment includes a decay spectroscopy station (DSS) (Rajabali et al., 2013), which was used for decay-assisted laser spectroscopy of ^{204}Fr (Lynch et al., 2014) as well as for laser-assisted decay spectroscopy of ^{206}Fr (Lynch et al., 2016). During the 2014 campaign, a beam of ^{219}Fr was delivered to the DSS as part of the investigation and calibration of that setup (Billowes et al., 2014).

The CRIS DSS consists of a rotatable wheel hosting 10 thin carbon foils ($20\ \mu\text{g}\cdot\text{cm}^{-2}$ (Lommel et al., 2002)), an insulated copper foil for beam transport optimization, and a $50\ \text{Bq}\ ^{241}\text{Am}$ source for calibration. The implantation

position is surrounded by two silicon detectors: an annular surface barrier detector with an active area of $450\ \text{mm}^2$, thickness of $300\ \mu\text{m}$ and a hole with a 4 mm diameter for the beam to pass through, and a full passivated implanted planar silicon (PIPS) detector with an active area of $300\ \text{mm}^2$ and thickness of $300\ \mu\text{m}$ behind the foil. A close geometry is used to maximize the solid angle coverage with enough distance for the annular detector to minimize losses through the aperture. The full description of the DSS can be found in Rajabali et al. (2013).

The data were acquired with Xia DGF-4H modules on an event-by-event basis, which allows for an offline reconstruction of the event sequence and possible coincidences. The full data set is available in an online repository (Billowes et al., 2014).

2.2. IS637: Experimental campaign

The IS637 experiment consisted of two campaigns which took place in July and November 2018. This experiment aimed at analysing the production of francium, radium and actinium beams at ISOLDE, including ^{219}Fr .

The RIB is delivered directly to the ASET after the separator. ASET is a ladder-based system that combines charged particle and photon detectors to perform different types of decay-spectroscopy measurements. In this setup, the beam is implanted onto one of several thin substrates (foils) that are secured to a ladder, which can be vertically moved to different detector positions. The ASET features two silicon detectors for charged particles in a configuration similar to the CRIS DSS: an annular detector that faces the beam and thus allows it to be implanted on the substrate, and a full detector placed on the opposite side of the ladder (see Figure. 1). Both detectors are placed in a close geometry with the ladder, for the same reasons as described in the CRIS DSS setup in Section 2.1. During the IS637 campaign, the detectors used were an annular silicon surface barrier detector with an area of $450\ \text{mm}^2$, thickness of $300\ \mu\text{m}$ and a hole with a diameter of 6 mm, and a full PIPS with an active area of $300\ \text{mm}^2$ and thickness of $300\ \mu\text{m}$. The data acquisition system consisted of a CAEN V1724 module read out by the MIDAS software enabling event-by-event data collection and offline reconstruction of the coincident events. The implantation material used in this campaign were carbon foils with thickness of $20\ \mu\text{g}\cdot\text{cm}^{-2}$ (Lommel et al., 2002). The full data on ^{219}Fr are available in an online repository (Jajčičinová et al., 2018).

2.3. IS665: Experimental campaign

In August 2021 the IS665 experimental campaign was performed at ISOLDE with the purpose of measuring β -delayed fission of $^{176,178}\text{Au}$. Along the main experimental goal, a few measurements were made in order to study the half-lives of ^{215}At and ^{221}Ra . The full data on these isotopes are available online (Bara et al., 2021).

In the case of the ^{219}Fr measurement, a surface ionized RIB

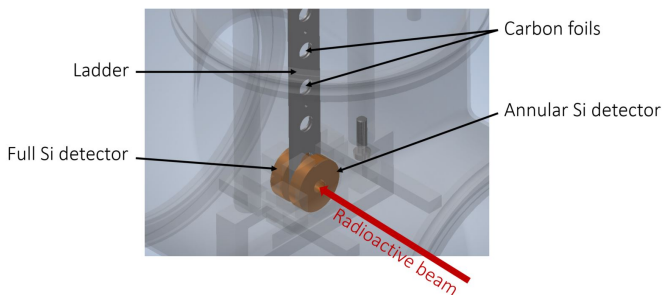


Figure 1: Schematic representation of the ASET. Annular detector placed in front while the incoming RIB is implanted into one of the foils hosted by the ladder. The full detector is placed behind the ladder.

was implanted continuously for about five minutes. In the case of ^{221}Ra , a molecular beam of RaF^+ with mass $A = 240$ was implanted. As explained earlier, this provides a pure beam of ^{221}Ra without possible contamination from the isobaric ^{221}Fr . In this case the beam was implanted for about three minutes; then the beam was stopped, but data acquisition continued in order to measure the unperturbed decay of ^{221}Ra as well.

For both implantations, ASET was used in the same experimental configuration as for the IS637 campaign, except that the annular detector featured an aperture of 8 mm instead of 6 mm for improved ion beam transport, and the full detector was a silicon surface barrier detector with an active area of 300 mm^2 . Both detectors had a depletion region thickness of $300\text{ }\mu\text{m}$ when fully biased. The acquisition system consisted of a CAEN N6730S module read out by the CAEN COMPASS software, recording event-by-event data allowing offline coincidence analysis.

3. Results

The short half-lives of ^{219}Fr and ^{215}At , of the order of ms and μs respectively, make the direct investigation of the ^{215}At half-life challenging. However, given the event-by-event nature of the data acquired in the campaigns described above, it is possible to reconstruct event sequences offline and to analyse the time difference between an α particle emitted from ^{219}Fr ($E_\alpha = 7312.3(18)\text{ keV}$), which acts as a reference for the production of ^{215}At , and an α particle emitted by ^{215}At ($E_\alpha = 8026.0(4)\text{ keV}$), which signifies the decay of the latter. The histogram of these time differences represents the decay curve of ^{215}At and allows an accurate determination of its half-life.

The limited implantation energy of the RIB, of 30-60 keV, compared to the energy of nuclear recoils (136 keV for ^{215}At after the decay of ^{219}Fr) results in the possibility for ^{215}At to be removed from the implantation foil. It may then either land on the surface of the annular silicon detector or recoil through its hole the detection of the α decay. Moreover, during the different campaigns, alignment difficulties for the DSS wheel or the ASET ladder resulted

in varying efficiencies for the detection of α particles between the upstream annular detector and the downstream full detector. Finally, timing issues in some of the data acquisition configurations resulted in de-synchronization of the detector read-outs. As such, each campaign could only apply selected coincidence configurations between either detector, as will be reported in this section.

The time distributions obtained for the events in coincidence in the different configurations were fitted with the following equation:

$$y = A \cdot e^{-\frac{\ln(2) \cdot t}{T_{1/2}}} + c, \quad (1)$$

where A (initial amplitude), $T_{1/2}$ (half-life) and c were the fitted parameters, the latter representing a constant background due to random coincidences. The fitting routine automatically takes the square root of the counts as uncertainty of the experimental points, unless the uncertainty carries additional information, such as when subtracting the background.

The case of ^{221}Ra is more straightforward, as it is sufficient to monitor the time behaviour of the intensity of its α lines to obtain the decay curve. Eventually, the activity of its progeny ^{217}Rn ($T_{1/2} = 0.54(5)\text{ ms}$) and ^{213}Po ($T_{1/2} = 3.72(2)\text{ }\mu\text{s}$) may be used as well, since they are in secular equilibrium with ^{221}Ra . To fit the curves obtained from the different α lines eq. 1 was used in this case as well, fixing the end of the implantation at $t = 170\text{ s}$.

Each data set was analyzed independently to allow a comparison of the findings. Nonetheless, a series of systematic effects were investigated, such as the impact of the binning, or of the fitting methods. Those are presented, with the complete datasets, in the supplementary material. We highlight below the global results from each campaign.

3.1. ^{215}At

3.1.1. IS471

The conditions from the IS471 campaign with the CRIS DSS resulted in low RIB intensity, which limited the statistics available for the analysis, but also prevented issues related to dead time, saturation or pile up. A typical α -decay energy spectrum is shown in Fig. 2.

The available coincidence configurations were with the ^{219}Fr α particle triggered in the full detector first and then the ^{215}At α particle detected in either the full or annular detector, or triggering from the annular detector and detected in the full detector. The annular-annular configuration could not be investigated. The three coincidence configurations were built and analyzed separately, by requiring an energy window around the respective α -decay peaks 4.25 times the full width at half maximum (FWHM). The time difference between the two α particles are monitored across $350\text{ }\mu\text{s}$, corresponding to about 10 half-lives. Random events are subtracted by monitoring the events where an α particle for ^{215}At is registered before the α particle from ^{219}Fr . Due to the limited statistics, the decay data are presented with $4\text{ }\mu\text{s}$ per bin to obtain enough statistics to produce meaningful fits.

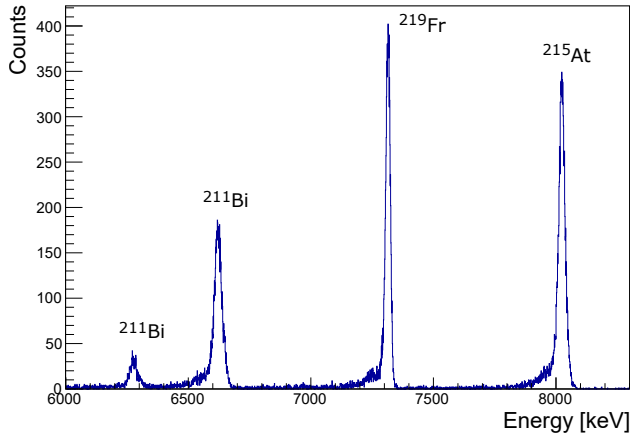


Figure 2: IS471: Typical α -decay energy spectrum for ^{219}Fr and its α -decay daughters, ^{215}At and ^{211}Bi . The bin size is 1 keV.

The decay curves were fitted using a maximum likelihood, given the limited statistics, according to Eq. 1, however with $c = 0$ as the spectra were background subtracted. The results obtained are presented in Table 1 and plotted in Fig. 3a). In order to calculate residuals, the difference between data and fit was divided by uncertainty of data.

3.1.2. IS637

For the IS637 campaign, a coincidence method was applied within the same detector for both the annular and the full detector, as electronic module desynchronization prevented the study of coincidences between different detectors. Given the dead time of the electronic modules of about $6 \mu\text{s}$, no coincidence data could be recorded in this time window, as can be identified on Fig. 3b). During offline analysis, the coincidences within the same detector were set from 1 to 15 expected half-lives ($37 \mu\text{s}$) time window and its effect on the fitted value was observed. The coincidences were made by starting with the detection of the ^{219}Fr α particle, followed by the detection of the ^{215}At α particle in the same detector. The energy gates were set to take a complete peak of the corresponding α particle. Equation 1 was applied for the fit of the final coincidence data set. In addition, the impact on the fitted half-life of other variables such as fitting range, energy window, and binning was examined and is presented in the supplementary material. The results are presented in Fig. 3b) and Table 1. The residuals were calculated the same way as for IS471.

3.1.3. IS665

During the IS665 campaign, the average counting rate of mass $A = 219$ in the α detectors was of the order of 10 kHz, but because of the short half-life of ^{219}Fr , the instantaneous rate right after the hit of the proton pulse on the target reached even 30-40 kHz. The directly produced ^{219}Fr would decay almost completely before the hit of the

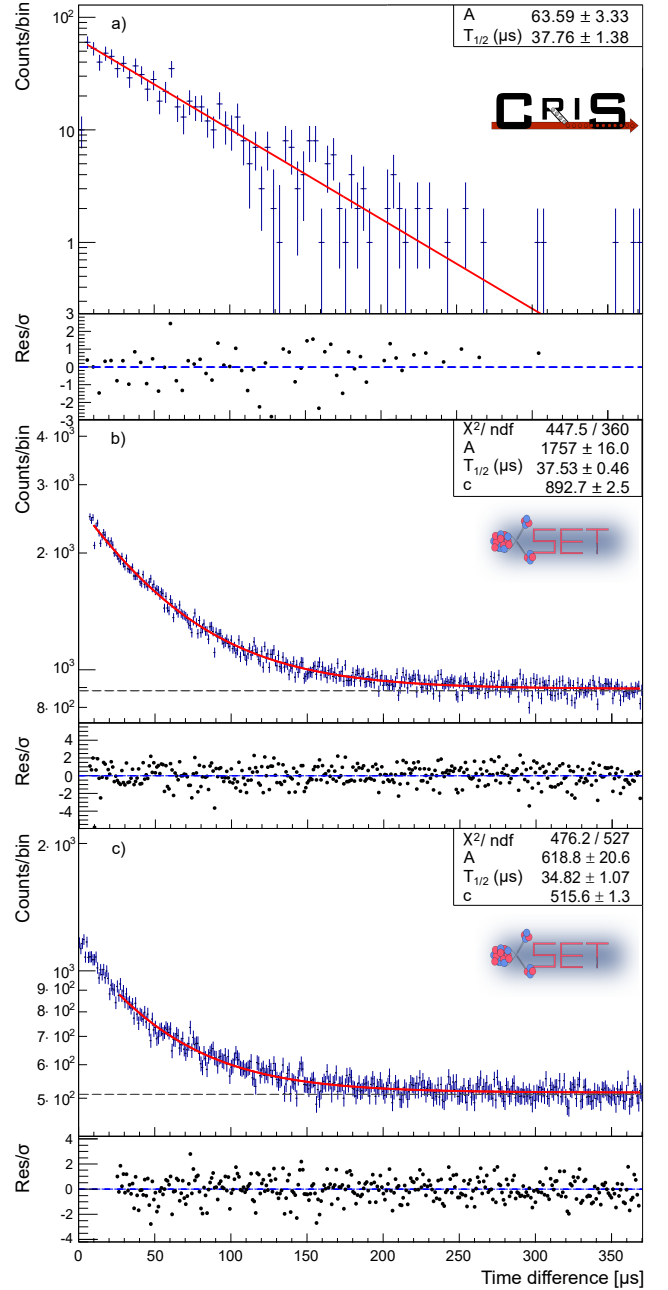


Figure 3: Half-life determination of ^{215}At based on the coincidence data from the **a)** Full-Full (IS471) **b)** Annular-Annular (IS637) **c)** Annular-Full (IS665) detector combination within coincidence window of $370 \mu\text{s}$. The bin size is $4 \mu\text{s}$ for a), and $1 \mu\text{s}$ for b) and c). The grey dashed lines represent the constant background. See text for details. The uncertainty of each data point is automatically considered to be the square root of the counts. In a) the uncertainty from the subtraction of the background is propagated automatically by the fitting routine. The residuals shown correspond to difference between data and fit, divided by uncertainty of data.

next proton pulse (since proton pulses are spaced by multiples of 1.2 s), but it was continuously fed in a lower rate by the α decay of ^{223}Ac accumulated in the target. As a consequence, a higher rate was concentrated in a very short

Table 1: ^{215}At half-life results obtained from the analysis of all three experiments. The "-" indicates the impossibility to perform coincidences. The uncertainty in "()" is the statistical one, while the systematic uncertainty is reported in "[]".

Detector combination	IS471 $T_{1/2}$ [μs]	IS637 $T_{1/2}$ [μs]	IS665 $T_{1/2}$ [μs]
Full - Full	37.8(14)[9]	36.5(5)[6]	-
Annular - Annular	-	37.5(5)[6]	-
Full - Annular	35.0(10)[9]	-	32.3(9)[9]
Annular - Full	37.5(9)[9]	-	34.8(11)[9]

period of time lasting about 700 ms after proton impact, creating a lot of pile-up and saturation events in the acquisition system. Moreover, some events were not properly identified as pile-up by the software COMPASS, resulting in consecutive events too close in time (with respect to the trapezoid filter time window) being assigned the same energy even though they should have been discarded. In order to avoid issues due to such spurious events, it was decided to select only the statistics beyond this 700 ms time after proton impact and up to the next proton pulse, and neglect the events too close in time. More details are presented in the supplementary material.

For the IS665 campaign, the time window used to create coincidences for half-life determination of ^{215}At was varied between 3 to 15 times the expected half-life of $37 \mu\text{s}$, in order to allow a good time range, but not to include too many random coincidences.

The plot in Fig. 3c) shows the decay curve obtained from the coincidences of the two different detectors. This was obtained gating on the α line of ^{219}Fr in the annular detector and on the α line of ^{215}At in the full detector. The fit was started from $25 \mu\text{s}$ in order to avoid the initial range that was affected the most by the pile-up and saturation problems. More details in the supplementary material.

Coincidences within the same detector were neglected given the amount of saturation and pile-up events caused by the high-instantaneous rates.

The results obtained from the different configurations are presented in Fig. 3c) and Table 1. The residuals were calculated the same way as for IS471. From the systematics studies performed on the influence of the different fitting parameters, systematic uncertainties were determined for each experimental campaign: $0.6 \mu\text{s}$ for IS637, and $0.9 \mu\text{s}$ for IS471 and IS665, see more details in the supplementary material.

3.2. ^{221}Ra

3.2.1. IS665

The procedure used to study the half-life of ^{221}Ra was simpler than the one used for ^{215}At . In fact, in this case the isotope of interest was directly implanted. To obtain the curve used to fit the half-life, it was sufficient to gate on the

time behavior of its α lines at $E_\alpha = 6607 \text{ keV}$, 6662 keV , 6754 keV . The α spectrum from the annular detector is shown in Fig. 4.

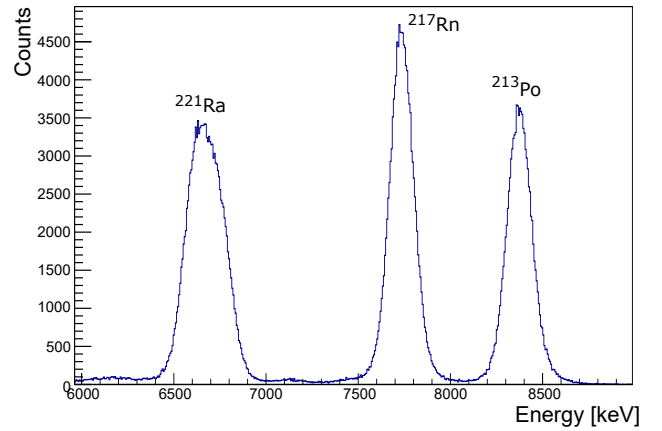


Figure 4: IS665: Typical α -decay energy spectrum for ^{221}Ra from the annular detector. The bin size is 1 keV.

The results obtained from the full detector are shown in Fig. 5. From the plot it is possible to distinguish the implantation part, up to about three minutes, and the following decay part. The latter was fitted using Eq. 1.

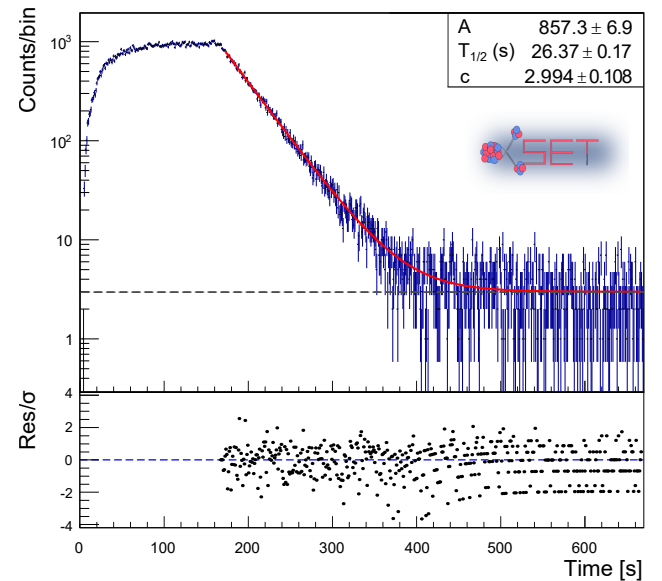


Figure 5: Total curve obtained by gating on the ^{221}Ra α line in the full detector from implantation of ^{221}Ra . The first part (up to about 3 minutes) represents the implantation, followed by the decay in the second part. The bin size 1 s. The red line represents the fitting function. The grey line corresponds to the constant background. The residuals shown correspond to difference between data and fit, divided by uncertainty of data. The structures in the residuals plot that can be observed from 400 s onwards are an effect due to the choice of the bin size on discrete number of counts.

The α -decaying daughter and granddaughter of ^{221}Ra are ^{217}Rn ($T_{1/2} = 0.54(5) \text{ ms}$, $E_\alpha = 7738(3) \text{ keV}$) and ^{213}Po

Table 2: ^{221}Ra half-life results obtained from the IS665 experiment with either detector and monitoring the α -decay line from ^{221}Ra , ^{217}Rn , and ^{213}Po . The uncertainty in "()" is the statistical one, while the systematic uncertainty is reported in "[]".

Origin	^{221}Ra $T_{1/2}$ [s]	^{217}Rn $T_{1/2}$ [s]	^{213}Po $T_{1/2}$ [s]
Full	26.37(17)[50]	26.67(22)[70]	26.32(20)[55]
Annular	26.00(18)[55]	26.27(19)[57]	25.99(18)[49]

($T_{1/2} = 3.72(2) \mu\text{s}$, $E_\alpha = 8376(3) \text{ keV}$), respectively. The α lines of both these isotopes were present in the α spectra, and since their half-lives are much shorter than the one of their precursor, they are already in secular equilibrium with ^{221}Ra at the end of implantation, and they follow the same time behavior as the ^{221}Ra . By gating on their α lines, it is possible to deduce the half-life of ^{221}Ra , as presented in Table 2. Similarly to the ^{215}At case, a systematic uncertainty was determined for each α gate in each detector, and it varied between 0.23 and 0.58 s, see the supplementary material for more details.

4. Discussion

In spite of their differences, the three campaigns presented very consistent results in the study of the half-life of ^{215}At , as can be seen in Fig. 6. All the results are also in very good agreement with the revised half-life measured by S amark-Roth et al. (2018) but with a higher precision. The weighted average of the seven measurements reported in Table 1, give a value of $36.3(3) \mu\text{s}$. Including also the systematic uncertainty of $0.9 \mu\text{s}$, the final half-life of ^{215}At from these combined data is therefore $36.3(3)[9] \mu\text{s}$, compared to $37(3) \mu\text{s}$ (S amark-Roth et al., 2018) or $100(20) \mu\text{s}$ (Meinke et al., 1951).

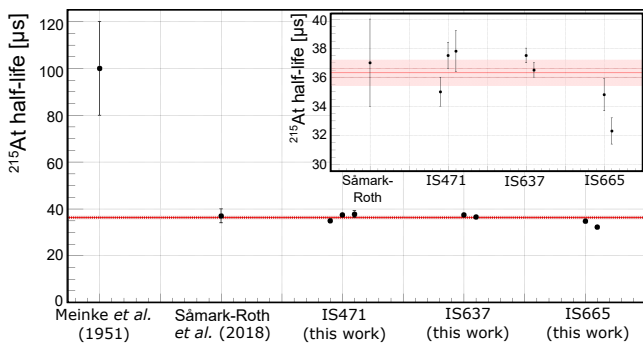


Figure 6: Comparison between the different ^{215}At half-life determinations in this work and in literature (Singh et al., 2013; S amark-Roth et al., 2018). The red line represents the weighted average value obtained from all the results of the campaigns described in this work. The dashed lines represent the limits given by the statistical uncertainty, while the full band is the region covered by the systematic uncertainty. The inset provides a better view of the results from this work and from S amark-Roth et al. (2018).

The ^{221}Ra half-life obtained from the two detectors, using also events from the daughter and granddaughter, are presented in Fig. 7, compared to the previous literature values (Meinke et al., 1951; Tove, 1958). The weighted average of both values gives a half-life of $26.2(1) \text{ s}$. Two different values of systematic uncertainty were found from the two silicon detectors used (0.5 s and 0.6 s from the annular and from the full detector, respectively), and the highest was taken for the final value, $26.2(1)[6] \text{ s}$.

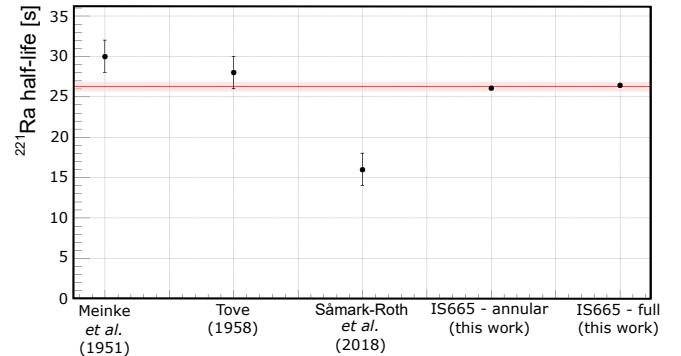


Figure 7: Summary of the fitted values for the ^{221}Ra half-life compared to the literature values (S amark-Roth et al., 2018; Kumar Jain et al., 2007). The red line shows the average value obtained from the IS665 campaign data. The statistical uncertainty falls completely under the thickness of the average line, and the full band is the region covered by the systematic uncertainty.

Unlike the results obtained for the ^{215}At half-life, the value found for the half-life of ^{221}Ra in this work does not agree with the $16(2) \text{ s}$ reported S amark-Roth et al. (2018). It agrees instead with the $28(2) \text{ s}$ reported in literature previously (Meinke et al., 1951; Tove, 1958), though with increased precision.

Using the newly determined half-lives, the reduced α decay widths (δ_α) were calculated for a wide range of Po, At, Rn, and Ra isotopes in the region using the formalism of Rasmussen (Rasmussen, 1959), assuming no change in angular momentum. Only ground-state-to-ground-state decays were considered for isotopes with $N = 127 - 135$, where neutrons and protons occupy the large valence space above ^{208}Pb giving rise to smoothly changing collective behaviour. The input data (α -decay energy, half-life, branching ratio) were taken from the literature (Basunia, 2022; Singh et al., 2013; Wu, 2007; Kondev et al., 2018; Singh et al., 2019, 2021; Browne and Tuli, 2011; Kumar Jain et al., 2007; Singh et al., 2011; Browne, 2001; Singh and Singh, 2015; S amark-Roth et al., 2018) or from this work. Note that for ^{216}Ra , both the evaluated half-life of $187(10) \text{ ns}$ and the recently measured half-life of $161(11) \text{ ns}$ (Sun et al., 2017; Parr et al., 2019) are considered.

Alpha-decay hindrance factors (HF) are then computed by comparing those δ_α , between At and Po isotones on the one hand, and between odd- A and even- A Ra isotopes on the other (Van Duppen and Huysse, 2000).

The δ_α of even- N isotopes of Po, At, and Rn are presented in Table 3a and shown in Fig. 8. The Po and At trends are

Table 3: a) Reduced α decay widths (δ_α) of even- N $_{84}\text{Po}$, $_{85}\text{At}$, $_{86}\text{Rn}$ isotopes and b) hindrance factors of the At isotopes against Po. For ^{215}At , the δ_α and HF are calculated using the half-life value obtained from our measurement.

N	δ_α $_{84}\text{Po}$ [keV]	δ_α $_{85}\text{At}$ [keV]	δ_α $_{86}\text{Rn}$ [keV]
128	70(1)	72(4)	89(8)
130	108(1)	116(4)	184(24)
132	119(1)	124(2)	183(3)
134	117(1)	135(21)	176(1)

(a)

N	HF $_{85}\text{At}$
128	1.0(1)
130	1.1(1)
132	1.1(1)
134	1.2(2)

(b)

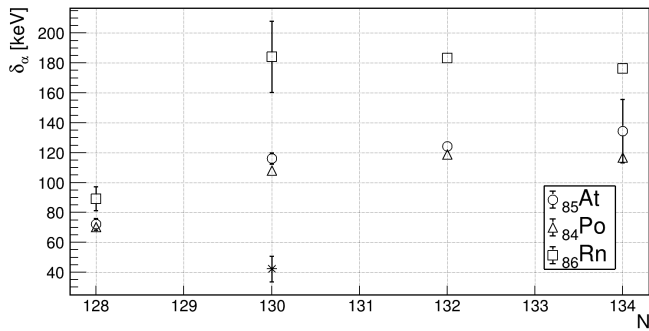


Figure 8: Reduced α decay widths (δ_α) of the even- N Po, At, and Rn isotopes in the range $N = 128 - 134$. The point indicated with a star corresponding to ^{215}At , calculated with the half-life of $100(20) \mu\text{s}$ from Meinke et al. (1951), shows a big deviation from the trend of the other isotopes.

very similar, while the trend in Rn shows a sudden increase in the partial decay width at $N = 130$. This corresponds to where energy density functional theory predicts the onset of octupole deformation in the region, as shown for Ac in the work of Verstraelen et al. (2019) (see their Fig. 6). It was thus decided to only use the Po isotones as reference for the calculation of the HF of At, presented in Table 3b.

The HF of At are also shown in Fig. 9. The HF value of $0.39(8)$ determined with the literature half-life of $100(20) \mu\text{s}$ shows a substantial departure from the trend of the other At isotones, while the HF determined with the half-life from this work is very consistent with the other isotopes.

The δ_α of the Ra isotopes are presented in Table 4a. The HF are calculated with respect to the interpolated value between the two nearest even-even Ra isotopes and given in Table 4b. The typical HF between even- A and

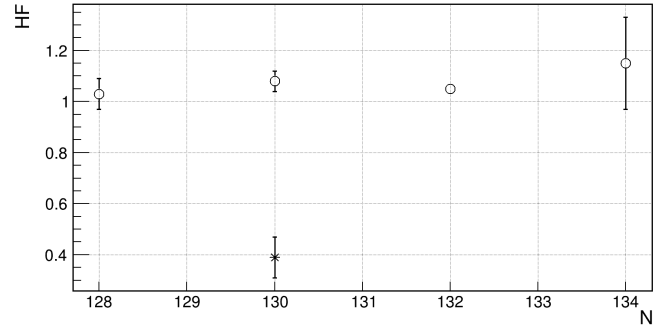


Figure 9: Hindrance factors of the even- N At isotopes with respect to their Po isotones in the range $N = 128 - 134$. For ^{215}At , the HF determined from our measurement is shown with an open symbol and the HF determined from Meinke et al. (1951) is shown with a star.

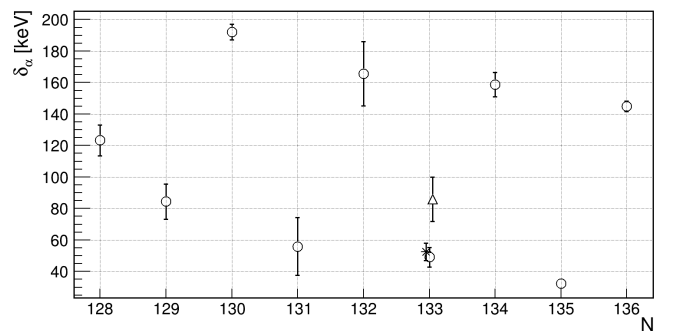


Figure 10: Reduced α decay widths (δ_α) of the Ra isotopes in the range $N = 128 - 135$. For ^{221}Ra , the δ_α determined from our measurement is shown with a star and the δ_α determined from the literature half-lives is shown with an open symbols, the circle for the value from Meinke et al. (1951) and the triangle for the value from Smark-Roth et al. (2018).

odd- A isotopes of even- Z elements is around 3. We observe here that the HF for $^{219}\text{Ra}_{131}$, $^{221}\text{Ra}_{133}$, and $^{223}\text{Ra}_{135}$ are consistent with this, provided we consider the longer half-life from this work rather than that from Smark-Roth et al. (2018). However, the HF of $^{217}\text{Ra}_{129}$ is < 2 , similar to the value calculated for $^{221}\text{Ra}_{133}$ with the half-life from Smark-Roth et al. (2018). From the δ_α trends in Fig. 10, one may see that the δ_α of $^{216}\text{Ra}_{128}$ is breaking from the trend of the heavier isotopes, which is probably highlighting a change of structure while approaching $N = 126$.

5. Conclusion

The half-life of ^{215}At has been revisited through three separate campaigns at ISOLDE, using beams of ^{219}Fr . A value of $36.3(3)[9] \mu\text{s}$ is deduced, which confirms a recent measurement from GSI TASCA but has a higher precision. Furthermore, the half-life of ^{221}Ra was measured directly thanks to the use of molecular beams of RaF^+ . A value of $26.2(1)[6] \text{s}$ is deduced, in agreement with the literature (Tove, 1958) but in disagreement with the GSI TASCA result (Smark-Roth et al., 2018), and with improved pre-

Table 4: Reduced α decay widths (δ_α) of $_{88}\text{Ra}$ isotopes and hindrance factors of the odd- A isotopes against even- A isotopes. For ^{221}Ra , δ_α and HF using the literature value for the half-life and the one obtained from our measurement (*) are presented for comparison, as well as the value obtained using the half-life from S amark-Roth et al. (2018) (**).

N	δ_α $_{88}\text{Ra}$ [keV]	N	HF $_{88}\text{Ra}$
128	123(1)	129	1.9(3)
129	84(11)	131	3.2(1)
130	192(5)	133	3.3(6)
131	56(18)		3.1(5)(*)
132	166(20)		1.9(4)(**)
133	49(6)	135	4.7(3)
	52(6)(*)		(b)
	86(14)(**)		
134	159(8)		
135	32(1)		
136	145(3)		

(a)

cision.

The new half-lives were used to determine α -decay hindrance factors for ^{215}At and ^{221}Ra , that are well in line with the systematics of α -decay hindrance factors in this region of the nuclear chart.

Autorship contribution statement

S. Bara: Writing – review & editing, Writing – original draft, Investigation, Formal analysis, Data curation. **E. Jaj c isinova:** Writing – review & editing, Writing – original draft, Investigation, Formal analysis, Data curation. **T. E. Cocolios:** Writing – review & editing, Writing – original draft, Supervision, Investigation, Formal analysis, Data curation. **B. Andel:** Investigation, Writing – review & editing. **S. Antalic:** Writing – review & editing. **A. Camaiani:** Investigation, Writing – review & editing. **C. Costache:** Investigation, Writing – review & editing. **K. Dockx:** Data curation, Investigation, Formal analysis. **G. J. Farooq-Smith:** Writing – review & editing. **A. Kellerbauer:** Investigation, Writing – review & editing, Supervision. **R. Lica:** Investigation, Writing – review & editing. **K. M. Lynch:** Investigation, Writing – review & editing. **P. Marini:** Investigation, Writing – review & editing. **M. Piersa-Silkowska:** Investigation, Writing – review & editing. **S. Stegemann:** Investigation, Writing – review & editing. **M. Stryjczyk:** Investigation, Writing – review & editing. **D. Treasa:** Investigation, Writing – review & editing. **P. Van Duppen:** Writing – review & editing, Supervision

Acknowledgements

The authors would like to acknowledge all those who participated in the data collection at the CRIS experiment and with the ASET. Furthermore, we would like to thank the ISOLDE Collaboration and technical teams for providing excellent beams and the GSI Target Laboratory for the carbon foils used in all these campaigns.

This work has received funding from the FWO-Vlaanderen (Belgium), KU Leuven (STG/15/031, C14/22/104), and FWO and F.R.S.-FNRS under the Excellence of Science (EOS) programme (grant no. 40007501); from the Science and Technology Facilities Council grants ST/G006415/1, ST/L005794/1, ST/L005786, ST/P004423/1, and Ernest Rutherford Grant no. ST/L002868/1; from the European Union Seventh Framework through ENSAR(506065); from the ERC Consolidator grants no. 648381 (FNPMLS), no. 771036 (ERC CoG MAIDEN), and no. 101088504 (NSHAPE); from the European Union’s Horizon 2020 research and innovation programme under grant agreement no. 642889 (MEDICIS-Promed); from the Romanian IFA grant CERN/ISOLDE and Nucleu project no. PN 23 21 01 02; from the Scientific Grant Agency VEGA (Contract No. 1/0651/21) and Slovak Research and Development Agency (Contract no. APVV-18-0268); from the Academy of Finland (project

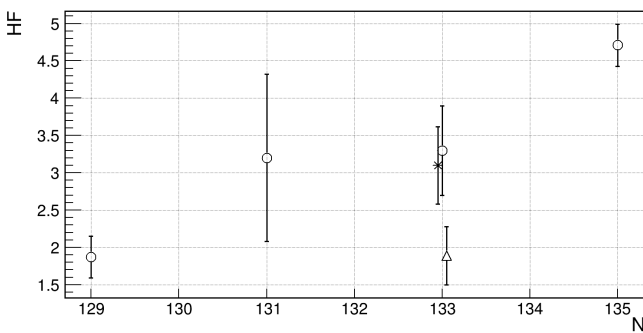


Figure 11: Hindrance factors of the odd- A Ra isotopes with respect to their even- A neighbors in the range $N = 127 - 135$. For ^{221}Ra , the HF determined from our measurement is shown with a star and the HF determined from the literature half-lives is shown with an open symbols, the circle for the value from Meinke et al. (1951) and the triangle for the value from S amark-Roth et al. (2018).

No. 354968).

This work was supported by the Collaborative Doctoral Partnership between Joint Research Centres of the European Commission no. 35332 between JRC Karlsruhe and KU Leuven. S.B. acknowledges the support of the FWO Fellowship. M.P.S. acknowledges the funding support from the Foundation for Polish Science (FNP). We would like to thank Jake Johnson and Hilde De Witte for the fruitful discussions on the data acquisition and analysis of the IS665 data.

References

- W. W. Meinke, A. Ghiorso, G. T. Seaborg, Artificial chains collateral to the heavy radioactive facilities, *Physical Review* 81 (1951) 782–798.
- G. Graeffe, P. Kauranen, The α decay of ^{219}Fr and ^{215}At , *J. Inorg. Nucl. Chem.* 28 (1966) 933–936.
- G. Bastin, C. F. Leang, R. J. Walen, Etude des niveaux de ^{220}Fr , ^{219}Fr , ^{216}At et ^{215}At , *J. Phys. Colloques.* 29-C1 (1968) 181–182.
- A. Sámárk-Roth, et al., Low-lying states in ^{219}Ra and ^{215}Rn : Sampling microsecond α -decaying nuclei, *Phys. Rev. C* 98 (2018) 044307. URL: <https://link.aps.org/doi/10.1103/PhysRevC.98.044307>. doi:10.1103/PhysRevC.98.044307.
- B. Singh, et al., Nuclear data sheets for A=215, *Nuclear Data Sheets* 114 (2013) 2023–2078.
- P. A. Tove, Alpha-emitters with short half-life induced by protons on heavy elements, *Arkiv Fysik* 13 (1958) 549.
- A. Kumar Jain, S. Singh, S. Kumar, J. K. Tuli, Nuclear data sheets for A=221, *Nuclear Data Sheets* 108 (2007) 883–992.
- M. D. Sun, et al., New short-lived isotope ^{223}Np and the absence of the $Z = 92$ subshell closure near $N = 126$, *Phys. Lett. B* 771 (2017) 303–308.
- E. Parr, et al., α -decay spectroscopy of the $N = 130$ isotones ^{218}Ra and ^{220}Th : Mitigation of α -particle energy summing with implanted nuclei, *Phys. Rev. C* 100 (2019) 044323.
- K. Valli, An experimental investigation of the alpha fine structure in ac-225, fr-221, at-217, and po-213, *Ann.Acad.Sci.Fennicae* (1964) Ser.A VI, No.165.
- J. D. Johnson, et al., Resonant laser ionization and mass separation of ^{225}Ac , *Scientific Reports* 13 (2023) 1347.
- M. Au, et al., In-source and in-trap formation of molecular ions in the actinide mass range at CERN-ISOLDE, *Nucl. Instrum. Meth. B* 541 (2023) 375–379.
- T. E. Cocolios, et al., The collinear resonance ionization spectroscopy (CRIS) experimental setup at CERN-ISOLDE, *Nucl. Instrum. Meth. B* 317 (2013) 565–569.
- R. P. de Groote, et al., Use of a continuous wave laser and Pockels cell for sensitive high-resolution collinear resonance ionization spectroscopy, *Phys. Rev. Lett.* 115 (2015) 132501.
- K. T. Flanagan, K. M. Lynch, et al., Collinear resonance ionization spectroscopy of neutron-deficient francium isotopes, *Phys. Rev. Lett.* 111 (2013) 212501.
- I. Budinčević, et al., Laser spectroscopy of francium isotopes at the border of the region of reflection asymmetry, *Phys. Rev. C* 90 (2014) 014317.
- M. M. Rajabali, K. M. Lynch, et al., A dedicated decay-spectroscopy station for the collinear resonance ionization experiment at ISOLDE, *Nucl. Instrum. Meth. A* 707 (2013) 35–39.
- K. M. Lynch, et al., Decay-assisted laser spectroscopy of neutron-deficient francium, *Phys. Rev. X* 4 (2014) 011055.
- K. M. Lynch, T. E. Cocolios, et al., Combined high-resolution laser spectroscopy and nuclear decay spectroscopy for the study of the low-lying states in ^{206}Fr , ^{202}At , and ^{198}Bi , *Phys. Rev. C* 93 (2016) 014319.
- J. Billowes, et al., IS471 - Decay spectroscopy data from the CRIS francium campaign 2014, DOI: 10.5281/zenodo.8262790, 2014.
- B. Lommel, W. Hartmann, B. Kindler, J. Klemm, J. Steiner, Preparation fo self-supporting carbon thin films, *Nucl. Instrum. Meth. A* 480 (2002) 199–203.
- E. Jajčičinová, et al., Open dataset for publication: Half-life determination of ^{215}At and ^{221}Ra with high-purity radioactive ion beams - IS637, DOI: 10.5281/zenodo.8262524, 2018.
- S. Bara, et al., Open dataset for publication: Half-life determination of ^{215}At and ^{221}Ra with high-purity radioactive ion beams - IS665, DOI: 10.5281/zenodo.8262560, 2021.
- J. O. Rasmussen, Alpha-decay barrier penetrabilities with an exponential nuclear potential: even-even nuclei, *Phys. Rev.* 113 (1959) 1593–1598.
- M. Basunia, Nuclear data sheets for A=213, *Nuclear Data Sheets* 181 (2022) 475–585.
- S.-C. Wu, Nuclear data sheets for A=216, *Nuclear Data Sheets* 108 (2007) 1057–1092.
- F. Kondev, et al., Nuclear data sheets for A=217, *Nuclear Data Sheets* 147 (2018) 382–458.
- B. Singh, et al., Nuclear data sheets for A=218, *Nuclear Data Sheets* 160 (2019) 405–471.
- B. Singh, et al., Nuclear data sheets for A=219, *Nuclear Data Sheets* 175 (2021) 150–268.
- E. Browne, J. Tuli, Nuclear data sheets for A=220, *Nuclear Data Sheets* 112 (2011) 1115–1161.
- S. Singh, et al., Nuclear data sheets for A=222, *Nuclear Data Sheets* 112 (2011) 2851–2886.
- E. Browne, Nuclear data sheets for A=215,219,223,227,231, *Nuclear Data Sheets* 93 (2001) 763–1061.
- S. Singh, B. Singh, Nuclear data sheets for A=224, *Nuclear Data Sheets* 130 (2015) 127–182.
- P. Van Duppen, M. Huyse, Shape coexistence around the $Z = 82$ closed shell probed by α -decay, *Hyperfine Interac.* 129 (2000) 149–161.
- E. Verstraelen, et al., Search for octupole-deformed actinium isotopes using resonance ionization spectroscopy, *Phys. Rev. C* 100 (2019) 044321.